JGR Solid Earth

RESEARCH ARTICLE
10.1029/2021JB023530

# Biased Witnesses: Crystal Thermal Records May Give Conflicting Accounts of Magma Cooling

**C. Culha[1], T. Keller[2], and J. Suckale[1]**

[1]Department of Geophysics, Stanford University, Stanford, CA, USA, [2]School of Earth and Geographical Sciences, University of Glasgow, Glasgow, UK

**Key Points:**

- Crystals in convection preserve the least information about the most dynamic flow domain
- Crystals in convection show signs of dissolution, suggesting a slower than actual cooling rate
- Crystals can record cooling, heating, and complex thermal histories even during steady cooling

**Correspondence to:**

C. Culha,
cculha@stanford.edu

**Citation:**

Culha, C., Keller, T., & Suckale, J. (2022). Biased witnesses: Crystal thermal records may give conflicting accounts of magma cooling. *Journal of Geophysical Research: Solid Earth*, *127*, e2021JB023530. https://doi.org/10.1029/2021JB023530

Received 30 OCT 2021
Accepted 15 APR 2022



**Abstract** Crystals retain an imprint of the dynamic changes within a magma reservoir and hence contain invaluable information about the evolving conditions inside volcanic plumbing systems. However, instead of telling a single, simple story, they comprise overprinted evidence of numerous processes relating to temperature, pressure and composition that drive crystal precipitation and dissolution in magmatic systems. To decipher these different elements in the story that crystals tell, we attempt to identify the observational signatures of a simple, yet ubiquitous process: crystal precipitation and dissolution during magma cooling. To isolate this process in a complex magmatic system with intricate dynamic feedbacks, we assume that synthetic crystals precipitate and dissolve rapidly in response to deviations from thermodynamic equilibrium. In our crystalline-scale simulations, synthetic crystals drag along the cooler-than-ambient melt in which they precipitated and can drive a temperature-dependent, crystal-driven convection. We analyze the non-dimensional conditions for this coupled convection and record the heterogeneous thermal histories that synthetic crystals in this flow regime experience. We show that many synthetic crystals dissolve, loosing their thermal record of the convection. Based on our findings, we suggest that heterogeneity in the thermal history of crystals is more indicative of local, crystal-scale processes than the overall, system-wide cooling trend.

**Plain Language Summary** Similar to tree rings, crystals tell a story of their past through their sequential growth records. However, unlike trees, crystals are dynamic and can travel throughout the magmatic domain. We hypothesize that this mobility may result in a bias in the crystal record and prevent it from accurately recording the magma reservoir history. In order to understand what patterns natural sample crystals would record during cooling, we built a simulator that tracks individual crystals and the thermal environment they experience. We simulate how crystals drive flow, but also precipitate and dissolve in response to temperature change. Our results show that each synthetic crystal has a unique record of its past that is dependent on the temperature distribution within its vicinity. Additionally, most of the synthetic crystals dissolve in the convection, so we lose their record. Overall, the synthetic crystals in our simulation can reproduce some of the variable patterns that are often found in natural samples, suggesting that real crystals are imperfect witnesses of the magmatic dynamics they are exposed to.

## 1. Introduction

Some volcanoes erupt with little or no clear warning, raising questions about which processes in the plumbing system trigger eruptions. Individual crystals in erupted samples may contain vital clues but deciphering these clues has proven challenging. Part of the challenge is the multi-scale nature of volcanic systems. At the system-scale of an entire eruption or a layer in a plutonic outcrop, temperature, composition, and pressure appear to be approximately homogeneous in many volcanic systems (Bachmann et al., 2002; Flynn & Mouginis-Mark, 1994; Whitney & Stormer, 1985). At the crystalline-scale, however, there is significant heterogeneity in the conditions individual crystals appear to have recorded. For example, even at the scale of a single hand sample, neighboring crystals may exhibit different records (Bachmann et al., 2002; Wallace & Bergantz, 2005). The motivation for this study is to identify how modeling can contribute to our ability to reconstruct a coherent story from heterogeneous crystal records.

Crystals grow or dissolve as a function of temperature ($T$), composition ($C$), and pressure ($P$) to maintain thermodynamic equilibrium with their surrounding magma, preserving a tabular history of the conditions in the volcanic plumbing systems over time (Cashman & Blundy, 2013; Ginibre et al., 2007; Wallace & Bergantz, 2005). Of these contributions, heterogeneity in temperature has attracted particular attention because it may relate to eruption

triggering mechanisms. Some studies have argued that reverse zonations suggest fresh injections of hotter, more mafic melt into cooler, more felsic, crystal-rich magma reservoirs (e.g., Bachmann et al., 2002; Cashman & Blundy, 2013; Murphy et al., 2000; Shane & Smith, 2013). Others suggest that thermal zonations indicate latent heat release due to crystallization driven by degassing under decompression (Blundy et al., 2006) or evolving temperatures driven by system-scale thermal convection (e.g., Singer et al., 1995).

Thermal convection was one of the first hypotheses proposed to explain crystal heterogeneity (e.g., Bachmann et al., 2002; Huber et al., 2009; Murphy et al., 2000; Singer et al., 1995), but large, low-viscosity magma reservoirs were envisioned to sustain convection through thermal expansivity alone. While not impossible, recent studies of plutons highlight that melt-rich magma bodies likely exist as ephemeral, thin lenses within a larger—and much more viscous—crystal-rich mush zone (e.g., Cashman et al., 2017). Also, geologic evidence like mafic enclaves and schlieren features in intermediate to felsic igneous rocks (e.g., Alasino et al., 2019; Barbey et al., 2008) suggest incomplete magma mingling following a mafic recharge (Cheng et al., 2020; Davidson & Tepley, 1997; Sparks et al., 1977; Zellmer et al., 2003). One way of reconciling these two points of view could be crystal-driven convection, which allows for more rapid, if incomplete mixing even in relatively small melt-rich lenses (Culha et al., 2020).

The goal of this paper is to quantify the thermal histories that crystals experience during magma cooling in a melt-rich magma lens by coupling flow dynamics and crystal precipitation and dissolution. We focus on the Stokes-flow limit in which viscous effects dominate over inertia and crystals interact over spatial distances exceeding their own diameter by several orders of magnitude through the fluid they displace when moving. These long-scale hydrodynamic interactions can lead to collective behavior at scales much larger than individual crystals (Culha et al., 2020; Mucha et al., 2004; Segre et al., 2001). We hypothesize that the collective settling of crystals is associated with crystalline-scale heterogeneity in the thermal conditions that crystals experience and record unless they dissolve over the course of the dynamics.

To test our hypothesis, we develop a process-based numerical simulator in which flow drives synthetic crystal precipitation or dissolution and the presence of synthetic crystals drives flow. The simulations capture the hydrodynamic interactions between crystals and melt at the scale of individual crystals while tracking the thermal evolution and allowing for temperature-dependent crystal precipitation and dissolution. We calculate phase equilibria with evolving temperature using rhyolite-MELTS (Ghiorso & Gualda, 2015; Gualda et al., 2012), assuming a constant bulk composition in the interest of isolating thermal from compositional effects. Our simulation setup represents a hot, crystal-free magma emplaced in a cool magma reservoir. Crystals denser than melt precipitate near the cooling interface and settle collectively, thereby sustaining a crystal-driven downwelling of cool, crystal-rich magma that sinks into the hot injection layer, driving a coupled convection.

Our approach complements prior modeling efforts (e.g., Cheng et al., 2020) that have also investigated crystalline records but have focused on a crystal-rich environment. Volcanic systems span a range from largely fluid to largely solidified states at different depths and times. The physical processes governing these two limits, fluid dynamics as opposed to granular mechanics, are sufficiently distinct to merit different modeling approaches. Here, we focus on the melt-rich limit, where crystals are highly mobile, interact with each other over long spatial distances, and play an active role in driving flow. As a consequence of their mobility, they sample different temperatures relatively quickly, leading to crystal precipitation and dissolution. Once they are locked up in a mush, crystals still play an important role in the dynamics, but primarily through the load-bearing network they form (Bergantz et al., 2015), as characterized by coordination number and fabric tensors (Bergantz et al., 2017), rather than through their individual trajectories and hydrodynamic interactions. Partial growth and the presence of different chemical components in the interstitial fluid between crystals hence gain much more importance.

Another important difference between our work here and prior studies (Andrews & Befus, 2020; Cheng et al., 2020) is that we focus on the observational signature of steady cooling at the system-scale. In contrast, Cheng et al. (2020) use simulations to forecast the variable synthetic crystal zonations of a system-scale, external disruption introduced by the injection of a batch of crystal-free magma into a largely crystalline mush. Andrews and Befus (2020) focuses on precipitation and dissolution of plagioclase in a batch of stagnant magma experiencing decompression over time. While their model captures valuable details in terms of the specific crystal shape and size, it ignores magma dynamics and with it the dynamic role that crystals may play in driving or blocking flow, particularly in the fluid-rich limit. Our approach is complementary by focusing on identifying the

imprint of magma dynamics on the crystalline record and would lend itself to an integration with Andrews and Befus (2020).

Our simulations demonstrate that synthetic crystals experience variable thermal histories even during steady cooling at the system-scale. Variability at the crystal scale hence does not necessarily imply variability at the system scale. Synthetic crystals segregate from their adjacent melt and sample a spatially heterogeneous temperature field created by their collective impact on flow. This collective impact manifests in a crystal-driven convection flow field that dominates the heterogeneity in the thermal history experienced by neighboring crystals. Coupled convection can also lead to a preservation bias, because synthetic crystals that do not dissolve, originate in specific, non-random regions of the flow. This result suggests that mesoscale thermal heterogeneity in space can overprint broader system-scale trends, highlighting the challenges of deducing system-scale dynamics from individual crystal records.

We show that coupled convection forms when a crystal-rich downwelling develops faster than thermal diffusion advances. We identify the non-dimensional parameters that determine the onset of convection and its imprint on individual synthetic crystals. Our scaling analysis suggests that a crystal-driven form of thermal convection could occur in both mafic and felsic systems, depending on layer thickness, but would tend to be more common in mafic systems. This finding is consistent with thermal zonations being found both in felsic (Broxton et al., 1989; Couch et al., 2001; Waight et al., 2000) and in mafic systems like Hawaii and Stromboli (Kahl et al., 2011; Rae et al., 2016; Ruth et al., 2018). We also discuss other observational signatures of the coupled convection we identify that may be detectable in field data.

## 2. Methods

We formulate our model for the specific purpose of better understanding how crystal precipitation and dissolution interacts with temperature evolution and flow dynamics in a hot, melt-rich lens as it gradually cools over time. Our model focuses on the crystalline scale to be able to identify the imprint that the coupled flow leaves in the thermal histories of individual crystals. We intentionally choose a highly idealized, two-dimensional, square domain of hot magma exposed to a cool top boundary. This idealized setup is valuable, because it reduces the number of relevant scales and free parameters, but it implies that our process-based model is not directly applicable to any specific field site and does not accurately represent the intricate system-scale dynamics of magma lenses.

Our model is motivated by our evolving understanding of crystal magma storage (Cashman et al., 2017) as sketched in Figure 1a, where hot magma may get injected into a relatively cooler magma lens. Our model set up in Figure 1b zooms onto the upper interface within an idealized magma lens. To derive testable model predictions at the scale of individual crystals, we use a direct numerical simulation technique (Qin & Suckale, 2016; Suckale et al., 2012a) to resolve magma dynamics and use the rhyolite-MELTs software (Ghiorso & Gualda, 2015; Gualda et al., 2012) to model equilibrium phase relations and material properties as a function of temperature within our synthetic magma.

### 2.1. Governing Equations

We consider a closed model domain, $\Omega$, filled with an incompressible, viscous melt that contains $n$ synthetic crystals, $C_1$, $C_2$, $\ldots C_i \ldots C_n$, where $n$ evolves with temperature (see Section 2.2), but the crystal radius $a$ and mass $M_0$ are held constant. In the crystal-free portion of the domain, $\Omega / \cup_{i=1}^{n} C_i$, the melt velocity, $\mathbf{v}_\ell$, is continuous and momentum is conserved.

$$\nabla \cdot \mathbf{v}_\ell = 0, \tag{1a}$$

$$\rho_\ell \frac{\mathrm{D}\mathbf{v}_\ell}{\mathrm{D}t} = -\nabla p + \nabla \cdot \mu \left( \nabla \mathbf{v}_\ell + [\nabla \mathbf{v}_\ell]^T \right) + \rho_\ell \mathbf{g}, \tag{1b}$$

where $\mathbf{v}_\ell$ melt flow velocity, D/D$t$ is the material derivative, $\rho_\ell$ is the melt density, $p$ is the melt pressure, and $\mathbf{g}$ is gravity.

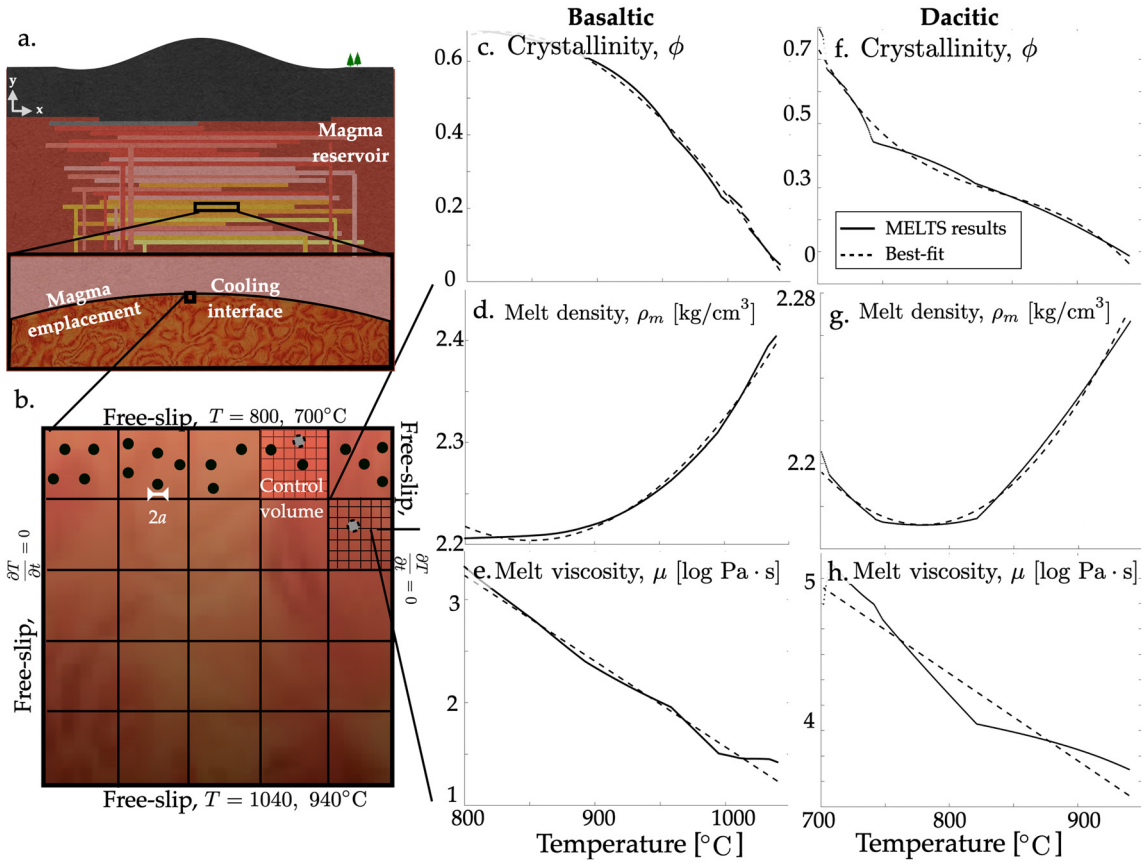


**Figure 1.** Rhyolite-MELTS results. We zoom into the cooling interface of an emplaced magma within a magma reservoir (a). We use basaltic and dacitic compositions to model phase equilibria for a range of temperatures at constant pressure to specify crystallinity (c) and (f), melt density (d) and (g) and melt viscosity (e) and (h) using the rhyolite-MELTS software. We update the crystallinity in each control volume of several grid cells by adding/removing crystals to match the calculated equilibrium, whereas we update the melt viscosity and density to their equilibrium value within individual grid cell (b). We use a different temperature range for basaltic composition from dacitic composition.

The motion of the synthetic crystals, modeled as rigid bodies, in the melt-free portion of the domain, $\cup_{i=1}^{n} C_i$, is driven by the balance between the gravitational force driving motion and the hydrodynamic force exerted by fluid resisting motion,

$$M\frac{d\mathbf{v}_i}{dt} = \mathbf{F}_i + M\mathbf{g}, \tag{2}$$

And the position of each synthetic crystals changes in accordance to their velocity, $\mathbf{v}_i$ arising from that force balance

$$\frac{d\mathbf{X}_i}{dt} = \mathbf{v}_i \tag{3}$$

where $\mathbf{X}_i$ is the location of synthetic crystal $i$ and $\mathbf{F}_i$ is the hydrodynamic force exerted by fluid resisting the motion of synthetic crystal $i$.

To resolve the long-range hydrodynamic interactions between synthetic crystal and melt phases, we use a customized, multiphase solver for magmatic systems that has been extensively benchmarked in previous studies (Qin et al., 2020; Qin & Suckale, 2016, 2017; Suckale et al., 2012a). We note that synthetic crystals also experience torque and could rotate in response to that (Qin et al., 2020), but this effect is negligibly small for spherical crystals and is neglected here in the interest of simplicity.

Unlike in a phase-average description of the Navier-Stokes equation, where the melt-crystal drag force density would be added to Equation 1b, we resolve the melt flow as a response to the presence of crystals. The crystals

can, by their buoyancy force, drive and, by their rigidity, redirect melt flow without needing an effective media model. The two domains, $\Omega / \cup_{i=1}^{n} C_i$ and $\cup_{i=1}^{n} C_i$, are coupled by enforcing a no-slip condition on all of the crystal interfaces, $\partial C_i$, which enforces that the velocity in the adjacent melt matches that of the synthetic crystal:

$$\mathbf{v}_\ell = \mathbf{v}_i \text{ on } \partial C_i \text{ for all crystals } i \in \{1, n\}. \tag{4}$$

We evaluate the hydrodynamic force, $\mathbf{F}_i$, acting on each synthetic crystal $i$ by integrating the flow field on $\partial C_i$. In addition to these $n$ internal boundary conditions emerging from the no-slip constraint, we impose free-slip on the domain walls

$$\frac{\partial \mathbf{v}_\ell}{\partial \mathbf{n}} = \mathbf{0}, \tag{5}$$

where $\mathbf{n}$ is the vector normal to the boundary. We set the grid size in our simulations based on the size of the synthetic crystals, such that a minimum of 4 grid cells fit within the diameter of the synthetic crystals. The crystals conserve momentum at the wall boundary, but the high viscosity slows the synthetic crystals such that they do not get into direct contact with the walls or with one another. For numerical stability reasons, there is a buffer of $2a$ size along the walls where synthetic crystals do not precipitate.

We compute the thermal evolution in the joint model domain, $\Omega$, including both the crystal-free and the melt-free subdomains. For simplicity, we ignore latent heat of crystallization, such that energy conservation reduces to an advection and diffusion equation for temperature:

$$\frac{\mathrm{D}T}{\mathrm{D}t} = \kappa \nabla^2 T. \tag{6}$$

We take thermal diffusion $\kappa = k/(\rho_\ell c_p)$, where heat capacity and conductivity of synthetic melt and crystal phases to be constant and the same at $c_p = 1367$ J/(K · kg) and $k = 1.53$ W/(m · K).

The top and bottom boundaries of the domain are isothermal. We take the hot interior and cold boundary temperature values for both compositions from Browne et al. (2006) as representative of typical mafic and felsic systems. The left and right walls are set to insulating $\left(\frac{\partial T}{\partial \mathbf{n}} = 0\right)$. We set the initial temperature profile as,

$$T\left(y, \tilde{t} = 750s\right) = \frac{(T_t + T_b)}{2} - \frac{(T_b - T_t)}{2} \mathrm{erf} \frac{(y - H)}{2\sqrt{\kappa \tilde{t}}} \tag{7}$$

where $T_t$ and $T_b$ are the initial top and bottom boundary temperatures, erf is the error function, $H$ is the domain height, $y$ is the vertical coordinate. The temperature distribution is initially uniform in the $x$-direction. Hence, the dynamic model sets in after heat has been lost diffusively for a time period $\tilde{t}$, an initial interval that would be nearly crystal-free and therefore without significant flow dynamics.

### 2.2. Modeling Temperature Dependent Magma Properties to Retain Equilibrium Conditions

In a dynamically evolving magma body (Figure 1a), crystal advection and the associated transport of temperature act to disequilibrate phase proportions locally. The natural system equilibrates by precipitating or dissolving crystals. In natural systems, there are multiple parameters that determine whether a crystal will precipitate or dissolve, including the availability of nucleation sites and necessary chemical components for precipitation, as well as the surface area of existing crystals for dissolution. Here, we focus only on the effect of temperature on crystal precipitation and dissolution as a first step toward a more complete model representation. Our algorithm instantaneously updates crystallinity to its equilibrium value in control volumes (CVs) that are 10 times larger than the synthetic crystal radius by randomly adding and removing crystals to the CV (Figure 1b).

We take the average temperature and crystallinity in the CV and compare to the equilibrium crystallinity as given by rhyolite-MELTS for the average CV temperature (Figures 1c–1h). In CVs where dynamic disequilibration has been detected, we enforce equilibrium by adding or removing synthetic crystals of constant and equal size at random positions within the CV until the crystallinity is within less than one crystal per CV of the equilibrium value. We refer to the removal and addition of synthetic crystals as "dissolution" and "precipitation" in the manuscript, respectively, but emphasize the simplified context in which we apply these terms here.

**Table 1**
*Model Compositions Based on the Average Compositions Sampled by the Unzen Eruption Described in Browne et al. (2006)*

| Comp. | $SiO_2$ | $TiO_2$ | $Al_2O_3$ | $Fe_2O_3$ | MnO | MgO | CaO | $Na_2O$ | $K_2O$ | $P_2O_5$ | $H_2O$ | T range |
|---|---|---|---|---|---|---|---|---|---|---|---|---|
| Basalt | 48.83 | 1.21 | 18.07 | 9.62 | 0.17 | 5.14 | 9.25 | 2.65 | 0.94 | 0.22 | 3.91 | 800–1040°C |
| Dacite | 63.92 | 0.62 | 15.16 | 0.82 | 0.08 | 2.04 | 4.28 | 3.47 | 2.52 | 0.17 | 3.87 | 700–940°C |

Inherent to this equilibrium transport approach is the assumption that precipitation and dissolution of crystals are more rapid than crystal advection. This is best justified for small crystals, which due to their high surface energy can rapidly grow from nucleation (Befus & Andrews, 2018; Brandeis & Jaupart, 1987; Toramaru, 2001) or rapidly and completely dissolve in undersaturated melt (Donaldson, 1985). Our assumption also implies the availability of sufficient nucleation sites and requires CVs that are small enough for chemical diffusion to keep pace with crystal and melt advection. The validity of rapid precipitation and dissolution decreases with increase in crystal size. However, even large crystals must have nucleated at a point in their history; our model can shed light on whether these long-lived crystals are likely to be representative samples.

In our simplified algorithm, we set the CV size to strike a balance between the objective to resolve small changes in crystallinity and the need to minimize numerical artifacts introduced by averaging. In Section 3, we provide a sensitivity analysis of the effect of CV size on our model results and find that it does not affect neither the overall flow dynamics nor the essential characteristics of temperature histories recorded by crystals, and it provides sufficient spatial resolution to capture the emerging flow morphology of crystal-driven convection.

While our choice of CV is motivated primarily by algorithmic considerations, it is supported by recent laboratory studies of particles in a viscous suspension exhibiting correlated flow over length scales of roughly $\sim 10a$ for a relatively wide range of particle fractions between 5% and 40% (e.g., Segre et al., 2001). This finding suggests that crystal interactions create correlated flow environments that are large as compared to crystal radius, but small as compared to the domain length. We assume that thermodynamic equilibration occurs on the same or a similar scale.

To set the material properties of crystal and melt phases, we reconstruct mafic and felsic end member cases using basaltic and dacitic compositions from Browne et al. (2006) (Table 1). We use their analyses of mafic enclaves and dacitic host magma, create a line of best-fit for each major oxide relative to $SiO_2$ content, use their reported $SiO_2$ content for the estimated basaltic and dacitic endmember compositions Browne et al. (2006) to reconstruct major element compositions, and finally normalize the resulting model compositions. We consider these two compositions mostly to highlight any general differences between coupled convection in mafic as opposed to felsic systems. Our study is not intended to accurately represent any one natural system.

We use the thermodynamic equilibrium solver rhyolite-MELTS (Ghiorso & Gualda, 2015; Gualda et al., 2012) to obtain equilibrium phase proportions by volume, melt density, melt viscosity, and the evolution of melt and crystal compositions with temperature for a given magma bulk composition (Table 1), pressure (200 MPa) and oxygen fugacity (Nickel-nickel oxide) at the liquidus. In Figures 1c–1h, we show the change in crystallinity, melt density, and dynamic viscosity for the mafic and felsic bulk compositions as a function of temperature together with best-fit polynomials which we use to more efficiently reference equilibrium crystallinity and melt properties in our magma dynamics simulations. For each composition, we consider a single, generic type of crystal that is denser than the melt phase. The crystals we model here are a few hundred $kg/m^3$ heavier than the host magma melt.

In addition to evolving crystal fraction with temperature, we also evolve melt density and viscosity with temperature. In real magma, crystal precipitation or dissolution depletes or enriches certain elements in the melt phase, which results in a change in melt density and viscosity. Similar to evolving crystallinity of the magma at the control volume scale using MELTs-rhyolite, we model the impact that crystal precipitation and dissolution, as well as temperature evolution have on melt density and viscosity as shown in Figures 1d–1h. We include these relations in the magma dynamics simulator by updating the density and viscosity at the scale of individual grid cells (Equation 1b).

### 2.3. Non-Dimensional Formulation

All of our simulations are dimensional because we link the magma dynamics to thermodynamics through MELTs, which is a dimensional software. To present our results, however, a non-dimensional analysis is valuable to identify the relevant scales and force balances governing the joint fluid mechanical and thermodynamic evolution of the flow.

To non-dimensionalize the governing equation we substitute all variables and parameters by characteristic scales multiplied to non-dimensional variables and parameters, with the former indicated by a subscript naught and the latter by a prime:

$$\begin{aligned} t &= t_0 t' & \nabla &= \nabla'/H \\ \mathbf{v}_\ell &= u_0 \mathbf{v}'_\ell & \mathbf{v}_i &= w_0 \mathbf{v}'_i \\ p &= p_0 p' & \mu_\ell &= \mu_0 \mu'_\ell \\ \rho_\ell &= \Delta\rho_0 \rho'_\ell & T &= \Delta T_0 T' \\ \mathbf{F_i} &= F_0 \mathbf{F}'_\mathbf{i} & M_i &= M_0 M'_i \\ \mathbf{g} &= g_0 \hat{\mathbf{z}} & \kappa &= \kappa_0 \kappa' \\ \mathbf{X}_i &= H_0 \mathbf{X}'_i. \end{aligned} \tag{8}$$

Note that we allow for different characteristic scales for the melt and crystal velocities, $u_0$, and $w_0$, respectively. Densities are scaled by the crystal-melt density difference scale, $\Delta\rho_0$. Temperature is scaled by the initial temperature difference across the domain, $\Delta T_0 = T_{\max} - T_{\min}$. We take $\kappa_0 = 10^{-7}$ m$^2$/s. Substituting these into the governing equations yields

$$\frac{u_0}{H_0} \nabla' \cdot \mathbf{v}'_\ell = 0, \tag{9a}$$

$$\frac{\Delta\rho_0 u_0}{t_0} \rho'_\ell \frac{\mathrm{D}\mathbf{v}'_\ell}{\mathrm{D}t'} = -\frac{p_0}{\ell'_0} \nabla' p' + \frac{\mu_0 u_0}{H_0^2} \nabla' \cdot \mu' \left( \nabla' \mathbf{v}'_\ell + \left[\nabla' \mathbf{v}'_\ell\right]^T \right) + \Delta\rho_0 g_0 \rho'_\ell \hat{\mathbf{z}}, \tag{9b}$$

$$\frac{M_0 w_0}{t_0} \frac{d\mathbf{v}'_i}{dt'} = F_0 \mathbf{F}'_i + M_0 g_0 \hat{\mathbf{z}}, \tag{9c}$$

$$\frac{H_0}{t_0} \frac{d\mathbf{X}'_i}{dt'} = w_0 \mathbf{v}'_i, \tag{9d}$$

$$\frac{\Delta T_0}{t_0} \frac{DT'}{Dt'} = \frac{\kappa \Delta T_0}{H_0^2} \kappa' \nabla'^2 T'. \tag{9e}$$

We choose some scales to be dependent, using classic choices for viscous flows where available: $u_0 = \Delta\rho_0 g_0 H_0^2/\mu_0$, the viscous speed at the domain scale; $t_0 = H_0/u_0$, the time scale of flow across the domain; $w_0 = \Delta\rho_0 g_0 a^2/\mu_0$, the viscous speed at crystal scale; $p_0 = \Delta\rho_0 g_0 H_0$, the buoyancy pressure at domain scale; and $F_0 = M_0 g_0$, the crystal buoyancy force scale. Using these as well as grouping terms, canceling scales where possible, and dropping primes gives.

$$\nabla \cdot \mathbf{v}_\ell = 0, \tag{10a}$$

$$\mathrm{Re}\, \rho_\ell \frac{\mathrm{D}\mathbf{v}_\ell}{\mathrm{D}t} = -\nabla p + \nabla \cdot \mu \left( \nabla \mathbf{v}_\ell + [\nabla \mathbf{v}_\ell]^T \right) + \rho_\ell \hat{\mathbf{z}}, \tag{10b}$$

$$\mathrm{ReRu} \frac{d\mathbf{v}_i}{dt} = \mathbf{F}_i + \hat{\mathbf{z}}, \tag{10c}$$

$$\frac{d\mathbf{X}_i}{dt'} = \mathrm{Ru}\, \mathbf{v}_i, \tag{10d}$$

$$\mathrm{Ra}\,\frac{DT}{Dt} = \kappa \nabla^2 T, \tag{10e}$$

where three linearly independent dimensionless groups of scales remain in the equations. These form dimensionless numbers including the Reynolds number,

$$\mathrm{Re} = \frac{\Delta\rho_0 u_0 H_0}{\mu_0} = \frac{\Delta\rho_0^2 g_0 H_0^3}{\mu_0^2}, \tag{11}$$

The crystal-driven Rayleigh number,

$$\mathrm{Ra} = \frac{\Delta\rho_0 g_0 H_0^3}{\mu_0 \kappa_0}, \tag{12}$$

And the ratio of crystal to melt speed scales,

$$\mathrm{Ru} = \frac{w_0}{u_0} = \frac{a^2}{H_0^2}. \tag{13}$$

The latter is a number characterizing the importance of phase segregation relative to system-scale convection in multi-phase flows (Keller & Suckale, 2019). Given the relatively high viscosity of magmatic systems, our simulations and respective results are within the Stokes limit described by $\mathrm{Re} \approx 0$.

The dynamics in these simulations arises from a form of double diffusion (Alsinan et al., 2017; Burns & Meiburg, 2015; Huppert & Sparks, 1988). Heat diffuses down gradients in temperature while crystals advect such that their collective motion can also be modeled as a diffusive process. Temperature diffusion causes crystals to form and dissolve. Crystal advection changes the local crystallinity and temperature field, since crystals drag the temperature field along as they advect. Thus, the two diffusive elements cause the system to behave as a temperature and crystallinity dependent, double diffusion (Huppert & Sparks, 1988), which can enhance or hinder classic processes like thermal convection or hindered settling. Furthermore, crystal-melt interactions introduce non-linear complexities within the collective flow that are not resolved in idealized mixture models (Keller & Suckale, 2019).

We are motivated to illustrate the affect these dynamics have on crystals, so for presenting our results below, we continue using the characteristic length as the domain height $H_0$ but select the crystal settling speed $w_0$ as the characteristic speed to scale model results. The characteristic time becomes $H_0/w_0 = t_0/\mathrm{Ru}$, such $t = 1$ would correspond to the time a single crystal would take to travel $H_0$ distance using a $w_0$. Non-dimensional temperature is shifted such that 0 and 1 correspond to the minimum and maximum temperatures in the domain, $(T - T_{\mathrm{min}})/(T_{\mathrm{max}} - T_{\mathrm{min}})$, with $T_{\mathrm{min}}$ set to 700°C and 800°C and $T_{\mathrm{max}}$ to 940°C and 1,040°C for felsic and mafic, respectively (Table 1). To present the temperature of a crystal, we average the temperature in the cells that contain the synthetic crystal. All of the simulations presented in this manuscript are provided in Table 2. The rest of the simulations used for grid convergence study and to identify relevant non-dimensional parameters, the simulation software and the input parameters can be accessed through our GitHub repository (Culha, 2022).

## 3. Results

### 3.1. Precipitation and Dissolution Processes Sustain Crystal-Driven Convection

To identify how crystal precipitation and dissolution alters the flow dynamics, we compare two simulations with mafic bulk compositions in Figure 2. In one of the simulations, we maintain equilibrium crystallinity by precipitating or dissolving synthetic crystals during flow (Figures 2a–2c). We reference this simulation as the "coupled" simulation. In the comparison case, we neglect equilibration by phase change and keep the number of synthetic crystals constant over time (Figures 2d–2f). We reference this simulation as "non-coupled". The coupled simulation varies in melt density and a viscosity as a function of temperature (Figures 1d and 1e). The non-coupled simulation assumes a constant melt density and melt viscosity.

**Table 2**
*Summary of Coupled Convection Experiments*

| Run Name | Figure | Final time | Ra | Ru |
|---|---|---|---|---|
| mafic-nc | Figures 2d–2f | $1.2 \times 10^{-2}$ | $5.7 \times 10^{4}$ | $1.0 \times 10^{-4}$ |
| mafic-c | Figures 2a–2c | $1.9 \times 10^{-2}$ | $5.7 \times 10^{4}$ | $1.0 \times 10^{-4}$ |
| mafic-big-c | Figure 3f&h; Figure 7 | $7.0 \times 10^{-3}$; $1.1 \times 10^{-2}$ | $1.5 \times 10^{6}$ | $1.1 \times 10^{-5}$ |
| Sim 1 | Figure 3a&c | $1.1 \times 10^{-2}$ | $1.5 \times 10^{3}$ | $4.0 \times 10^{-4}$ |
| Sim 2 | Figure 3b&d | $1.1 \times 10^{-2}$ | $1.5 \times 10^{3}$ | $1.0 \times 10^{-4}$ |
| Sim 3 | Figure 3e&g | $7.0 \times 10^{-3}$ | $1.5 \times 10^{6}$ | $1.0 \times 10^{-4}$ |
| Sim 4 | Figure 4c | $1.4 \times 10^{-2}$ | $5.7 \times 10^{4}$ | $1.0 \times 10^{-4}$ |
| Sim 5 | Figure 4i | $1.4 \times 10^{-2}$ | $5.7 \times 10^{4}$ | $1.0 \times 10^{-4}$ |
| felsic-c | Figure 5 | $3.0 \times 10^{-3}$ | $3.7 \times 10^{2}$ | $1.0 \times 10^{-4}$ |

*Note.* The simulations correspond to the coupled "c" and non-coupled "nc" simulations in this manuscript. All simulations follow the model conditions in Figure 1. The density difference at the crystalline scale is $7.8 \times 10^{2}$ kg/m$^3$ and $4.3 \times 10^{2}$ kg/m$^3$ for mafic and felsic simulations, respectively. The density difference we input for Ra number is 100 kg/m$^3$. The viscosity difference between mafic and felsic simulations is roughly $10^{2}$. We include a larger table of all runs in our git repository (Culha, 2020).

The synthetic crystals in both simulations settle under the joint influence of gravity and hydrodynamic forces. The crystal-scale hydrodynamic interactions are important dynamically because they lead to self-organization of the synthetic crystals into a collective flow pattern, as discussed for the magmatic context in Culha et al. (2020). In both simulations, the synthetic crystals initially drag cold magma along as they settle collectively. In the non-coupled simulation, settling of a fixed number of synthetic crystals leaves behind a gap in synthetic crystal distribution along the boundary. In contrast, precipitation replenishes crystallinity along the cooling boundary layer in the coupled simulation, forming a crystal-driven downwelling (Figures 2a and 2b) that grows into the

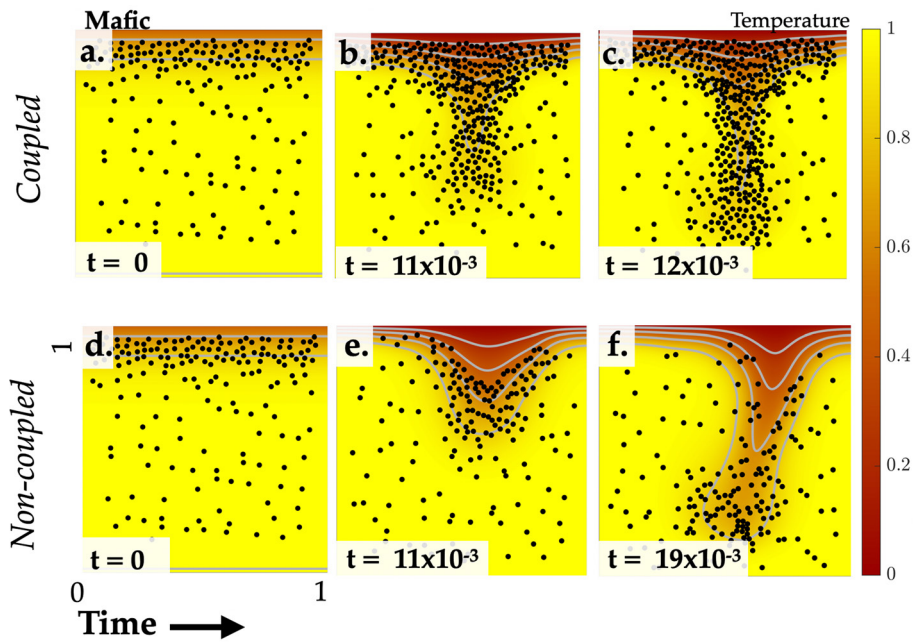


**Figure 2.** Coupling flow dynamics to thermal evolution and synthetic crystal precipitation/dissolution leads to a coupled convection. We show two simulations, one coupled (a–c) and one non-coupled simulation (d–f), where the initial number of synthetic crystals is left to evolve without precipitation/dissolution. Both simulations start with the same initial crystallinity and identical synthetic crystal positions.

downward current of an emerging convective cell (Figure 2c). The upward counter-flow current brings hotter, crystal-poor magma up toward the cooling boundary.

In the coupled simulation, synthetic crystals precipitate predominantly where the developing downwelling is advecting synthetic crystals away from the cooling boundary layer, thereby enhancing the downwelling and sustaining convective flow. The coupled convection advances synthetic crystals approximately twice as fast as the non-coupled convection (Figure 2). Although this enhances shuffling of synthetic crystals, the viscosity difference between the cool downwelling and the hot surrounding melt alters how temperature mixes in the coupled versus non-coupled convection (Figure 2). The temperature distribution at the downwelling interface in the coupled case in Figure 2b is sharper than in the non-coupled case in Figure 2e. The temperature gradients in Figure 2b are steeper than e, which is consistent with advection of temperature being relatively more important in coupled flow as compared to the more diffusive flow in the non-coupled model.

#### 3.1.1. Crystals in Convective Flow Exhibit Signs of Dissolution

To understand the consequences of coupled convection on the crystal cargo, we compare the thermal histories that crystals experience in coupled simulations without and with convection. Since coupled convection is a form of thermal convection, we suppress convective overturn in our simulation by reducing the Rayleigh number. The Rayleigh number represents the ratio between the time scales of diffusive to convective transport of temperature (Rayleigh, 1883) as defined in Equation 12. In contrast to classic Rayleigh-Bérnard convection, the density difference driving flow in our model is not the consequence of thermal expansion in the fluid or bulk density change, but of contrasts in synthetic crystal load.

Inclassic Rayleigh-Bérnard theory, convection occurs when Ra exceeds a critical value of $Ra_c \sim 10^3$ (Bergé & Dubois, 1984; Chandrasekhar, 2013; Drazin & Reid, 2004). In our case, $Ra_c$ does not strictly capture the regime boundary between statically conductive, and dynamically convective systems as in classic Rayleigh-Bérnard convection, because crystals settle even in the absence of crystal-driven convection. Despite our expectations on $Ra_c$, we test whether Ra reasonably predicts the regime transition from diffusion dominated to convective flow below. We also emphasize that we include the limit of very small domain sizes primarily to create a counterfactual for our simulations of coupled convection. Whereas magma lenses will tend to fall into the high Rayleigh number limit and motivates our interest in coupled convection, the low Rayleigh limit we show here could be representative of a thin horizontal sill.

In Figure 3, we compare four coupled simulations to illustrate how changing Ra and Ru affect the flow dynamics. We adjust Ra by changing domain size, $H$, and Ru by varying synthetic crystal size, $a$, while holding all other parameters constant. We show two simulations near the critical value of order $Ra_c \sim 10^3$ (Figures 3a and 3b), whereas two other simulations are well above at Ra of order $\sim 10^6$ (Figures 3e and 3f).

In Figures 3a and 3b, convection is suppressed and diffuse cooling progresses gradually from the top to the bottom as illustrated by the approximately horizontal isotherms (gray lines). However, the behavior is not identical in A and in B despite Ra being the same, because of variations in crystal-to system-scale speed ratio, Ru. In Figure 3a, with larger synthetic crystals and, hence higher Ru, the isotherms are slightly more curved and synthetic crystals are less homogeneously distributed than in Figure 3b. In contrast, Figures 3e and 3f both show convective overturn, but the exact flow patterns that emerge are clearly modulated by Ru in addition to Ra. Again, an increase in synthetic crystal size results in greater variance in the temperature distribution within the domain.

The histograms in Figures 3c–d and 3g–3H characterize the temperature change experienced by the synthetic crystal cargo in each of the simulations a–b and e−f, respectively. We record the thermal history of all synthetic crystals regardless of whether they escaped dissolution until the end of the simulation. We identify the temperature change of each of the synthetic crystals by recording its temperature at precipitation, as well as at the time of their dissolution or the stopping time of the simulation. We emphasize that our metric is not necessarily identical to the maximum temperature range of a synthetic crystal throughout its thermal history, because many synthetic crystals experience both cooling and heating temperature histories. We will return to this point in the next section.

We show a histogram of the temperature change for synthetic crystals that last until the end of the simulation in purple regardless of when they form, and of synthetic crystals that are dissolved prior to the stopping time in orange. Some of the synthetic crystals in the purple histogram may have entered a control volume that was out

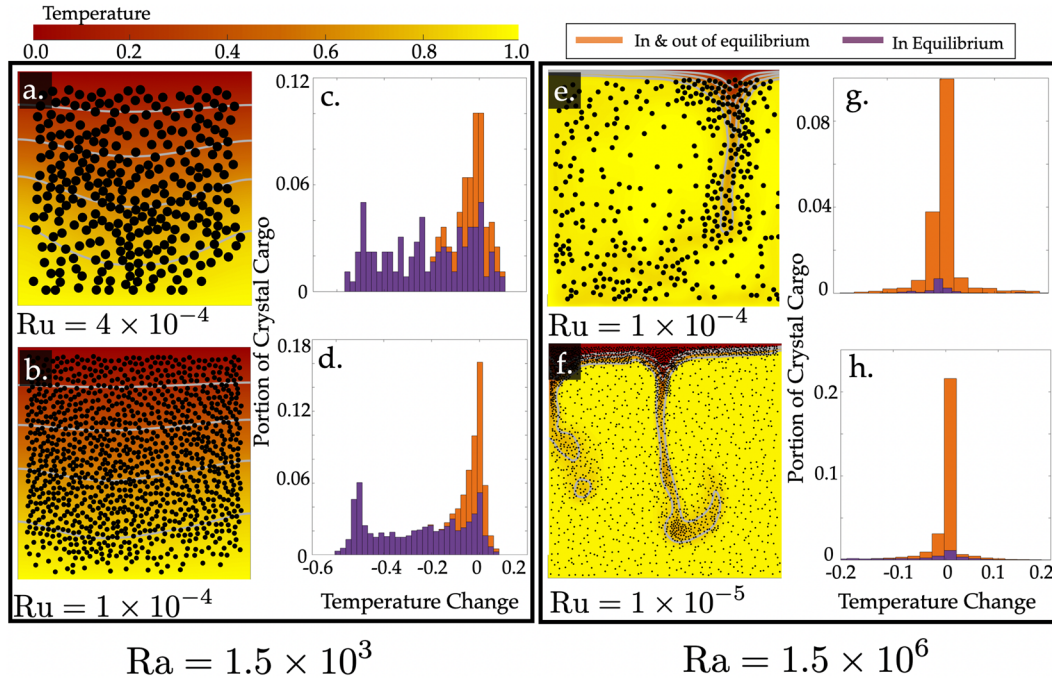


**Figure 3.** Implications of convection on crystal cargo. (a–d) and (e–h) are four simulations at two Ra and two Ru. (a–b) and (e–f) show simulation snapshots and (c–d) and (g–h) show what portion of the crystal cargo experience a certain temperature change, where positive and negative temperature change indicate heating or cooling, respectively. We show two crystal populations: In and out of equilibrium (orange) and out of equilibrium (purple).

of equilibrium, but were not randomly selected to be dissolved in our algorithm. We label the synthetic crystals depicted in the purple histogram as crystals "in equilibrium" and the ones in orange as crystals "in and out of equilibrium".

In the absence of convection, a significant portion of synthetic crystals (shown in purple Figures 3c and 3d) remain in equilibrium with the surrounding melt, while some (shown in orange) experience dissolution. In striking contrast, most of the synthetic crystals dissolve when the system is convecting, as indicated by the greatly diminished purple bars in Figures 3g and 3h. Also, most of the synthetic crystals experience a small change in temperature, suggesting that the crystals are shorter lived in coupled convection than at low Ra.

Since we enforce equilibration by temperature-dependent crystal precipitation/dissolution at the scale of the CV, we perform a sensitivity analysis to evaluate whether the overall flow dynamics or the temperature changes we infer for our synthetic crystals depend on CV size in Figure 4. We compare three different simulations at three different control volume sizes (a–c has CVs with $10 \times 10$ cells; d–f has CVs with $20 \times 20$ cells; and g–i has CVs with $30 \times 30$ cells). The CV sizes are illustrated in grid form in the middle panels (b, e, h). We measure our ability to resolve crystallinity changes with MELTS by taking the number of cells in a crystal (~16 cells) and dividing by the control volume size (100, 400, 900). As we mentioned in the Methods Section, increasing the CV size results in a better resolution of crystallinity, but can introduce numerical artifacts associated with averaging over a relatively large CV. We find that for our chosen CV size, we can resolve crystallinity changes of 4%, compared to 1.7% for the larger, and 8% for the smaller CV we compare against. We illustrate the averaging artifacts in Figure 4i, where the regions circled in cyan exhibit high crystallinity, as a consequence of averaging over a large CV, despite the local, relatively warm temperatures.

Regardless of the dynamics in panels C, F, and I varying slightly in terms of convection speed and downwelling morphology, the average temperature change experienced by individual crystals varies little for both "in equilibrium" and "in and out of equilibrium" crystals (see Figure 4j). Figure 4j shows the average recorded temperature change, similarly to the average recorded temperature change in histogram form in Figure 3. The vertical lines in Figure 4j signify the standard deviation about the average temperature. Although trumped by the variance, the

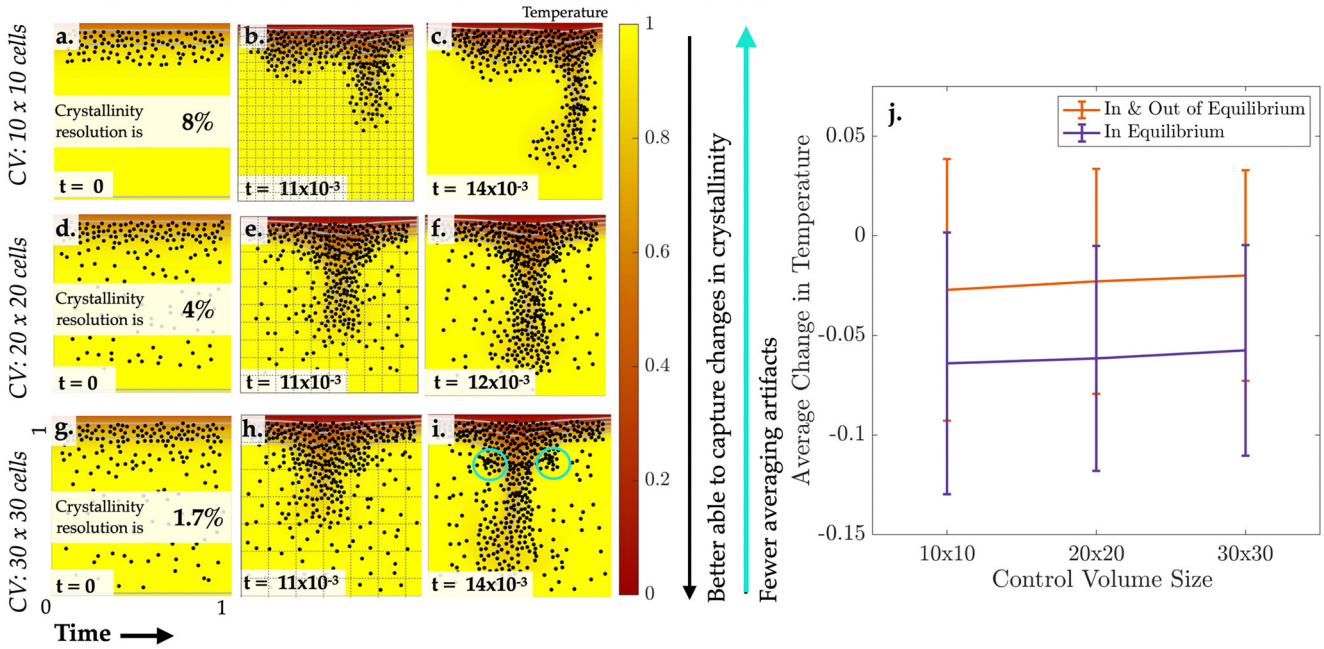


**Figure 4.** The role of control volume size. We test 3 different control volume sizes. a–c is 10 × 10 cells; d–f is 20 × 20 cells; and g–i is 30 × 30 cells. The middle column illustrates the size of the control volume. We quantify the crystallinity resolution, or the resulting sensitivity to crystallinity changes, in the first column. Cyan blue in (i) indicates the crystals that precipitated as a result of coarse control volume discretization. (j) is the average change in temperature (as calculated for Figure 3) for different control volume sizes.

average temperatures slightly increases with larger CV size, reflecting the fact that synthetic crystals can advect greater distances in larger CVs and can hence sample hotter temperatures before dissolving.

### 3.2. Crystals in Convection Preserve the Least Information

Our analysis raises the question how well synthetic crystals testify to dynamically evolving conditions within a magmatic system. In Figure 3, the orange histograms of dissolved synthetic crystals center around small temperature changes, whereas the purple histograms preserve a larger distribution of temperature changes. These results suggest that the synthetic crystals that escape dissolution tell a different story than the synthetic crystals that experienced disequilibration. We refer to this effect as preservation bias. It implies that certain parts of the flow are sampled by and recorded on our synthetic crystals, while other parts get omitted in the crystalline record of the convection.

Preservation bias is driven by advection and will hence be dominant in volcanic systems with a large Rayleigh number (see Section 3.1.1). This finding implies that preservation bias is less pronounced in high-viscosity magma as compared to low-viscosity magmas. To illustrate this difference, we compare a felsic (Figure 5) and a mafic simulation (Figure 6). In both cases, we split the simulation into five horizontal segments. At the end of each simulation, we select all the synthetic crystals in each of the segments and display their thermal history for their entire lifetime. The synthetic crystal records showing overall heating, cooling, or less than 10°C temperature change are displayed in red, blue, or gray, respectively.

In the coupled, felsic simulation (Figure 5), crystal advection rates are low (Ra = 370) and synthetic crystals sample the entire domain. Most crystals stay present throughout the entirety of the simulation. Of the 232 synthetic crystals that initially existed in the felsic simulation, 152, over 65%, remain present until the end. The rest of the synthetic crystals are lost due to small-scale reshuffling of crystals and in the hotter, bottom portion of the domain. The synthetic crystal records may be similar to well described processes like hindered settling (Burgisser et al., 2005; Dufek & Bergantz, 2005) in the absence of a system-scale flow field.

When crystal advection rates are high compared to thermal diffusion, as in Figure 6, synthetic crystals are not representative of the flow dynamics in either space or time. Of the 175 synthetic crystals that form and dissolve

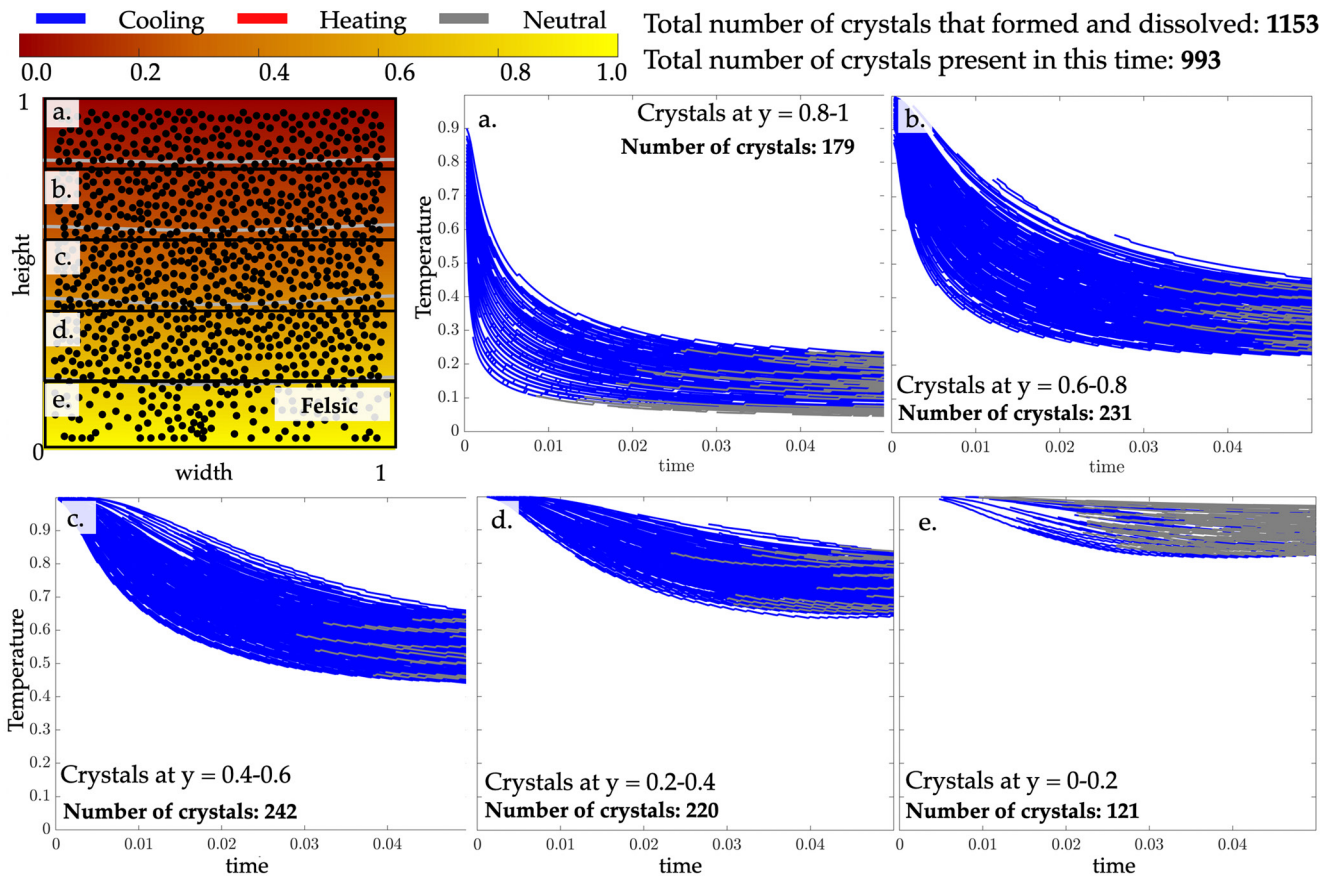


**Figure 5.** Representation in felsic synthetic crystal cargo analysis. The felsic composition, coupled simulation is split into different segments and the thermal history of the synthetic crystals that terminate in that segment are shown in plots (a–e). The blue and gray profiles suggest that the synthetic crystal experienced overall cooling and less than 10°C temperature change, respectively. Note that none of the crystals experience heating.

in the mafic, coupled simulation, 54, about 31%, remain present to the end of the simulation. Most of these preserved crystals remained at the top boundary, A. Since the cooler temperature at the top boundary increases melt viscosity locally, some of the synthetic crystals at the top of the downwelling move slower than the tip of the downwelling and cool with time (Figure 6a). This part of the domain is well sampled and documented by the synthetic crystals that remain in Segment A.

Information about the convective flow inside the emplaced magma is mostly lost, because many synthetic crystals are entrained in the downwelling and are subject to heating and dissolution, which means they are removed from the simulation (Figure 6b). Recording conditions at the tip of the downwelling could be valuable to identify the vigor of convection, but it is the least sampled portion of the domain and comprises of synthetic crystals with the shortest life span (Figures 6c–6e). Thus, most of the synthetic crystals in a coupled convection with high Ra preferentially record the least dynamic regions in a convecting melt lens (Figure 6a), rendering it challenging to reconstruct a coherent story from their records.

### 3.3. Crystals in Convection Show Evidence of Both Heating and Cooling

Despite imposing steady cooling at the system scale, only some of the synthetic crystals in the simulations with coupled convection record cooling while others record heating (Figures 3e–3h). Thus, some of the synthetic crystal records are consistent with the system-scale cooling trend, whereas others are not. In this section, we analyze how the thermal histories of synthetic crystals within the same and in different regions of the convective flow compare to one another. We do this analysis for the simulation in Figure 3f, because it contains many synthetic crystals in a large domain.

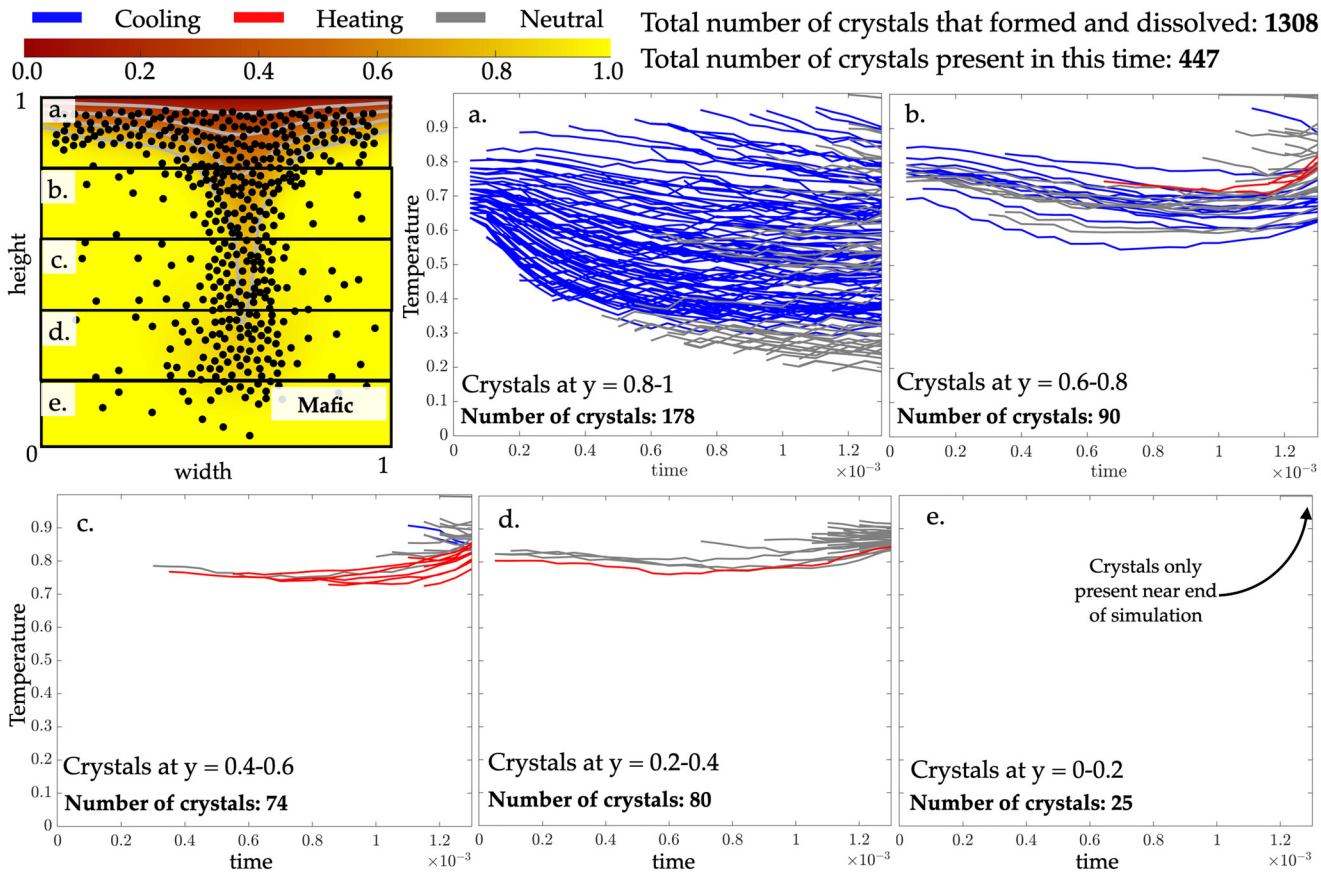


**Figure 6.** Bias in mafic synthetic crystal cargo analysis. We show the final snapshot of the simulation in Figures 2a–2c. The simulation domain is split into different segments and the thermal history of the synthetic crystals that terminate in that segment are shown in plots (a–e). The blue, gray and red profiles suggest that the synthetic crystal experienced overall cooling, less than 10°C temperature change, or heating, respectively.

To analyze a range of synthetic crystal histories evolving along distinct paths we select three sub-populations highlighted in blue, green and purple in Figure 7 and track their migration through the domain. The blue and green sub-population of synthetic crystals are initially positioned on the left and right sides of the cooling boundary layer, respectively, and remain within the top half of the domain over the course of the simulation. Purple crystals originate at the far left of the cooling boundary near the blue population but reach the base of the domain within the simulation time. The colored squares encapsulate all of the synthetic crystals in each of the sub-populations.

For each sub-population, we color a few synthetic crystals, which escape dissolution for the majority of the simulation. The simulation in Figure 7 shows that synthetic crystals that start in close proximity, such as some of the blue crystals, can travel to very different parts of the domain as a consequence of coupled convection. In the process, they may experience very different thermal histories. Conversely, synthetic crystals starting out in different segments of the domain can move close to one another and even intermingle, such as the green and blue crystals that are both being dragged into the downwelling in panel (c).

Figure 7d shows all temperature profiles within each sub-population to illustrate their variance. Our simulations show significant heterogeneity in the thermal histories of individual synthetic crystals. Some of the synthetic crystals experience continuous cooling or heating, while others first cool down before heating up again. Synthetic crystal histories are given as partially transparent lines, such that darker regions show where more than one synthetic crystal experienced the same temperature at the same time. Initially, dark blue and green patches around temperature of 0.65 show where blue and green crystals precipitate predominantly. They all first cool along a similar profile before their histories begin to diverge. The purple crystals precipitate at various times and at different temperatures, but then begin to converge to a heating profile, terminating at similar temperatures.

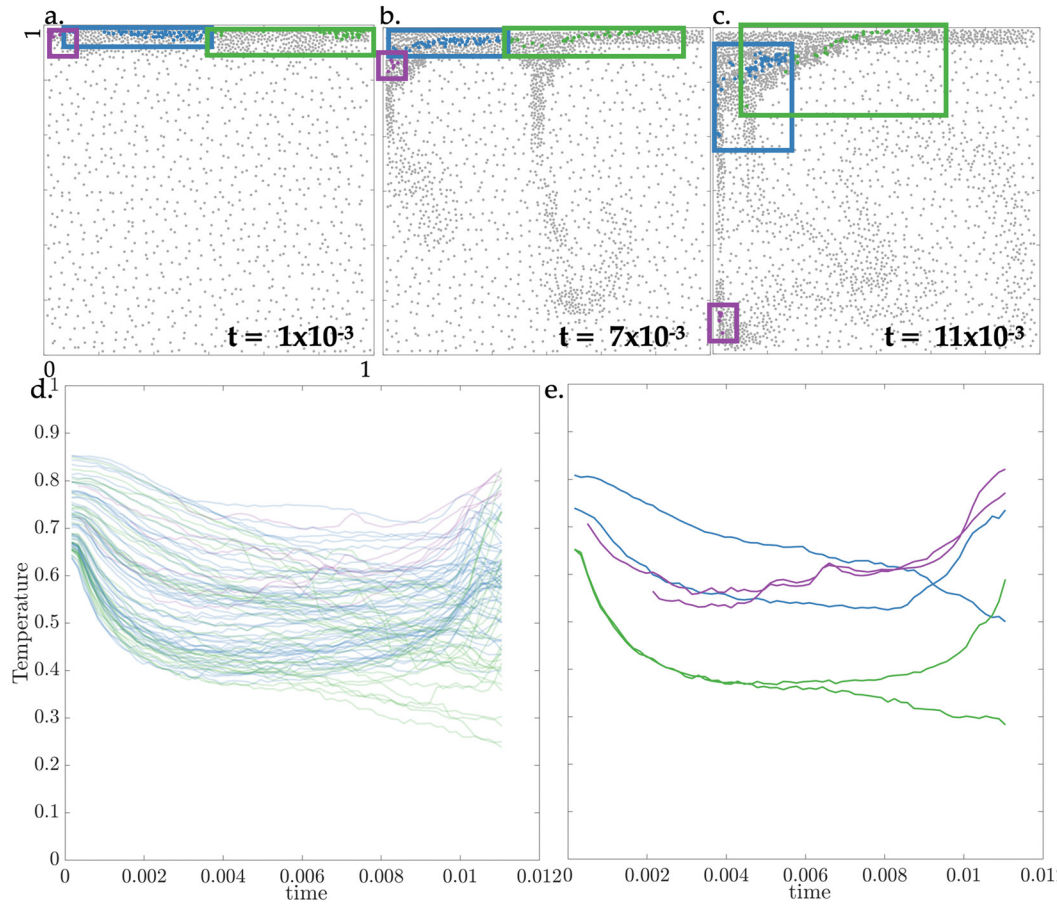


**Figure 7.** Neighboring crystals may show signs of crystals heating, cooling, or both. (a)–(c) shows snapshots of a simulation with same initial conditions as the simulation in Figures 2a–2c but 3× the size of that in Figures 2a–2c. We highlight three crystal sub-populations to show how synthetic crystals move together in some regions and separate in others. We color and analyze the crystals that escape dissolution for majority of the simulation. Purple crystals are synthetic crystals that traveled to the bottom of the domain over the course of the simulation. Blue and green crystals precipitated in the left and right sides of the top domain, respectively, and remained in the top half of the domain during the portion of the dynamics shown here. The square boxes focus on encapsulating all of the synthetic crystals in each category, and inevitably include some shorter lived crystals. (d) shows non-dimensional temperature profiles of the colored synthetic crystals from (a)–(c), where non-dimensional temperature 0 indicates 800°C and 1 indicates 1,040°C in our simulations from Figures 2a–2c. (e) shows two randomly selected profiles within each sub-population.

A closer look at a few randomly selected colored synthetic crystals (Figure 7e) emphasizes how analyzing only a few synthetic crystals may result in significantly biased representation of system-scale cooling. To demonstrate a scenario where only a few crystals in a handsample are analyzed, we show the detailed thermal crystal histories of two randomly selected synthetic crystals from each of the purple, blue and green sub-populations in Figure 7e. The selected crystals show a wide range of thermal histories. Some experience consistent cooling, namely one of the blue crystals in Figure 7e that exhibits a monotonic downward trend. Some crystals show consistent heating, such as the shorter lived of the two purple crystals.

The thermal history of some other crystals indicates both heating and cooling on relatively short timescales: Both of the two purple crystals show a small bump of heating and cooling. In addition, the longer-lived of the two purple crystals exhibits heating and cooling on long timescales. One of the green and one of the blue crystals provide evidence of a similar thermal history, capturing the temperature variations as the crystals move in and out of the main downwelling. This comparison of synthetic crystals from the same sub-populations shows that analysis of a few selected crystals even if found in close proximity in a handsample may show apparently conflicting evidence of system-scale evolution, because the crystals record the thermal history in their immediate vicinity

rather than at the system scale. Since crystals can drive flow and advect through different temperatures in the process, some sampled crystals may actually indicate heating within a steadily cooling magma lens.

## 4. Discussion

One of the fundamental challenges in volcanology is to infer the complex interwoven magmatic processes occurring at depth prior to eruption from limited data. Crystals trapped in magma quenched upon eruption record at least some aspects of the pre-eruptive conditions in the volcanic conduit directly (Demouchy & Mackwell, 2006; DiBenedetto et al., 2020; Spilliaert et al., 2006). However, leveraging crystal-scale data can be difficult since most volcanic models are formulated at the system-scale of hundreds of meters to tens of kilometers and do not entail testable model predictions at the crystalline-scale that could be tested against this data. Although the processes that we analyze here scale to larger domains (see Section 3.1.1), the model itself intentionally focuses on the crystalline scale and imposes several significant simplifications that is necessary to distill the complex interwoven process.

Recent modeling efforts indicate that incomplete sampling may bias the interpretation of crystal populations if there is substantial heterogeneity in the apparent thermal zonations they record (Andrews & Befus, 2020; Cheng et al., 2020). This is consistent with our model findings. In fact, our model shows that a potentially large portion of the crystals that nucleate could dissolve again before they have time to grow and develop thermal zonations. Since the flow systematically dissolves the crystals in the most dynamic portion of the flow field, preserved crystals contain the least information about the flow features, which are most pertinent to the system-scale thermal history. For example, convective overturn tends to be fastest during the early stages of cooling when temperature gradient is highest. The crystals that could provide testimony of this phase may not be preserved and the crystals that are available for analysis would suggest a shorter lived and less dynamic environment than was actually present.

The inability of crystals to provide accurate testimony of rapid convection raises the question whether there are any other observational indicators that would complement the inevitably incomplete crystal record. Our simulations suggest that one potential indicator of the coupled convection we identify here is the formation of crystal clusters. Synthetic crystals in a coupled downwelling congregate close to one another through "synneusis" (Culha et al., 2020; Schwindinger & Anderson, Jr., 1989; Vogt, 1921), the swimming together of crystals during flow. The long-range hydrodynamic interactions between crystals favor melt flowing around the cluster rather than through the individual narrow channels between crystals (Batchelor & Batchelor, 2000; DiBenedetto et al., 2020; Lamb, 1911; Qin & Suckale, 2020). The process is captured even in the non-coupled, mafic simulation in Figures 2d–2f. A distinct clusters forms at the bottom of the convection in Figure 2f.

In the coupled convection, hydrodynamically driven synneusis that form synthetic crystal clusters can further enhance crystallinity of a region, because synthetic crystals preferentially precipitate in crystal-rich regions along the top boundary and at the tail of the downwelling, where cooling and collective settling create favorable conditions (Figure 6). These synthetic crystal conglomerates (Figure 8d) resemble glomerocrysts in natural systems (Garcia & Jacobson, 1979) and hence could have implications on how such textures may form. The synthetic conglomerates preserve a thermal environment at their center that is distinct from the surrounding magma. Conversely, synthetic crystals along the outer rim would be most exposed to the dynamically changing thermal environment and would most likely experience heating (Figures 6c–6e). In natural glomerocrysts, this may translate into different geochemical environments depending on the relative location of the crystal within the glomerocryst. For example, crystals in the center may precipitate, sampling predominantly residual melt, whereas those near the outer rim of the natural glomerocryst may dissolve in the process of sampling new melt.

One more observable indicator of coupled convection may be cross-bedded crystal layers formed at the base of a cooling magma lens. Our model suggests that the tip of the crystal-rich downwellings may retain cool temperatures and the synthetic crystals associated with them for longer. After detaching from the tail of the downwelling, synthetic crystals are delivered to the base of the magma lens in batches (Figure 8e). Unlike crystals individually "raining" through the magma lens, the collective settling of crystals in multiple discrete crystal-rich batches would suggest a depositional environment similar to repeated gravity currents. This process could have contributed to cross-bedded crystal layers as observed at Duke Island, Skaergaard (Irvine, 1980) and Stillwater (Jackson, 1961) outcrops.

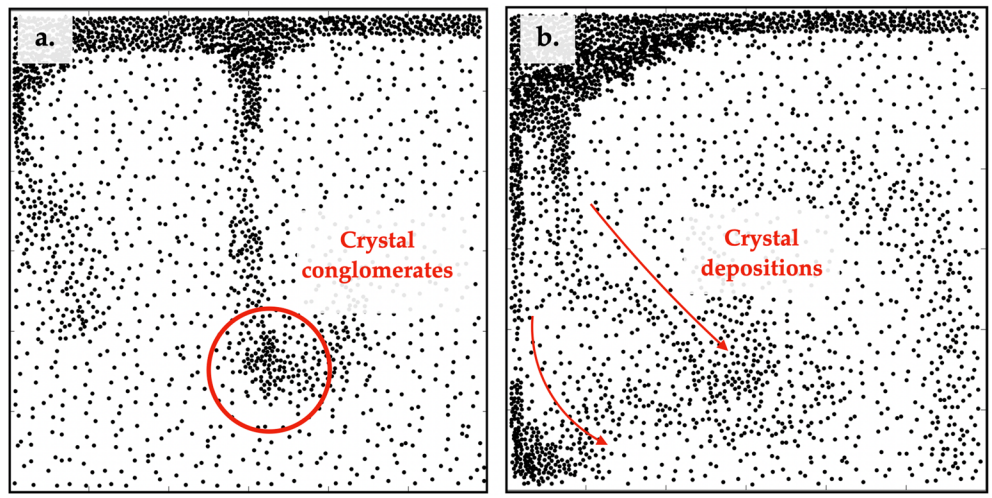


**Figure 8.** Indicators of coupled convection downwells. (a) is evidence of synthetic crystals precipitate preferentially near one another although surrounded by melt rich magma. Both precipitation and synneusis of synthetic crystals result in conglomerate formations that travel collectively through the melt, resembling glomerocrysts; (b) shows onset of multiple synthetic crystal depositions at the bottom of the domain which resembles the gravity currents.

We emphasize that our model is not designed to capture the complex, system-scale dynamics of any of these sites. Instead, the main contribution of our work is to identify the role that a simple, yet ubiquitous process—the precipitation and dissolution of crystals—plays in modulating the flow dynamics of thermal convection and how it is recorded by individual crystals. Our previous work (Culha et al., 2020) shows that crystal-driven convection alters convective processes such as thermal (Bachmann et al., 2002; Dufek & Bachmann, 2010; Huber et al., 2009; Murphy et al., 2000; Singer et al., 1995) or bubble-driven convection (Bergantz et al., 2017) by introducing collective flow behavior. In this study, we show that crystal-driven downwellings reflective of collective flow become self-sustaining when coupled to crystallinity evolving with temperature. Thus, thermodynamic phase changes are closely coupled with multi-phase transport dynamics as also observed in crystal-rich magmatic systems (Keller et al., 2017; Mittal & Richards, 2017).

The degree to which the coupled convection will enhance larger scale convection is dependent on how quickly crystals can respond to their evolving thermodynamic environment. Here, we make the simplifying assumption that thermodynamic equilibrium is instantaneously met each advective time step by precipitating new or dissolving existing crystals. In natural systems, the kinetics of crystal nucleation and partial precipitation or dissolution will inevitably add complexity (Kerr, 1995), such as increasing the size of the downwelling or changing the spacing between downwellings, leading to a more variable spectrum of coupled convective flow morphologies with a spectrum of downwelling speeds.

Our simulations provide a new perspective on the interpretability of crystal cargoes with heterogeneous crystal records where some crystals may show signatures of heating, cooling or both. We show that crystals record the thermal environment in their immediate vicinity, which could deviate significantly from the system-scale temperature evolution, particularly during coupled convection. Researchers have previously invoked large-scale, thermal convection, (e.g., Bachmann et al., 2002; Huber et al., 2009; Murphy et al., 2000; Singer et al., 1995), mafic injections (Annen et al., 2005), and magma mixing (Davidson & Tepley, 1997; Sparks et al., 1977; Zellmer et al., 2003) to explain crystal cargo heterogeneity in natural samples. We show here that no external, system-scale disruption is needed to explain a highly heterogeneous crystal cargo. Deducing system-scale dynamics from individual crystals is hence particularly challenging if systems experience convection, which our analysis suggests is likely particularly for large or low-viscosity magma lenses.

Recent literature on magma storage have looked at plagioclase and zircon crystals to understand timescales and temperatures of magma storage and notice surprisingly short timescales of magma storage in predominantly melt-rich, or hot, conditions (Cooper & Kent, 2014; Rubin et al., 2017). Given that we track our simulations from the reference frame of the domain and the synthetic crystals, we can compare what synthetic crystals would suggest

on simulation duration. The sub-populations of crystals in the more dynamic region of our domain (Figures 6b–6e) are shorter lived than the entire duration. For example, most of the synthetic crystals that survive to the end of the simulation in Figures 6d and 6e sample a tenth of the simulation duration. These synthetic crystals would suggest that the flow dynamics was hot and short lived in the sense that cooling started much later than it actually did. This may bias the interpretation of hot storage time to be much shorter than it actually was. Similarly, natural crystals may suggest short storage times if they precipitate well after magma emplacement.

## 5. Conclusion

Our analysis provides an example for how process-based models could contribute to deriving insights about magma dynamics from crystal records. By resolving the crystal–melt interactions within temperature dependent crystal load, we identify a self-sustaining form of double-diffusive convection driven by crystallization within a cooling boundary layer. The collectively settling crystals self-organize into meso-scale downwellings which drag cooler melt from the interface into the hotter magma below, resulting in a heterogeneous distribution of temperature, melt density, viscosity, and magma crystallinity throughout the magma lens. The main methodological contribution of our simulator is that it can track synthetic crystals and the thermal conditions that they sample, while allowing for synthetic crystal precipitation and dissolution. The synthetic crystal populations show a wide range of apparent thermal histories including heating and cooling. Moreover, we can keep record of the synthetic crystals that dissolve in our simulations, which make up the majority of the synthetic crystals entrained in the coupled downwelling. Hence, the crystal population left over from coupled downwelling does not provide a complete record of the flow dynamics that have occurred in the system. By better understanding the limits on the interpretation of crystalline data, we can improve our ability to quantify the longevity of hot storage regions, speed of remobilization, and rates of mafic injections that may drive eruptions. Our work emphasizes the significance of using multiple geochemical and textural indicators in magmatic systems to decipher the processes creating the real observable crystal records.

## Data Availability Statement

See our GitHub repository here for the Fortran simulator producing each case, some videos and the Matlab scripts that help generate the figures (Culha, 2022): https://doi.org/10.5281/zenodo.6482286.

**Acknowledgments**
The authors would like to thank Christy Till, Gail Mahood, Ayla Pamukcu, and David Pollard for fruitful discussions throughout the development of the project. This work is supported by NSF Grant 2048430 awarded to JS. CC acknowledges support from the NSF's GRFP, Stanford University's McGee Grant and Stanford University's Lieberman Fellowship. TK acknowledges support from the Swiss National Science Foundation's Postdoc.Mobility Fellowship 177816.

## References

Alasino, P. H., Ardill, K., Stanback, J., Paterson, S., Galindo, C., & Leopold, M. (2019). Magmatically folded and faulted schlieren zones formed by magma avalanching in the sonora pass intrusive suite, sierra Nevada, California. *Geosphere*, *15*(5), 1677–1702. https://doi.org/10.1130/ges02070.1

Alsinan, A., Meiburg, E., & Garaud, P. (2017). A settling-driven instability in two-component, stably stratified fluids. *Journal of Fluid Mechanics*, *816*, 243–267. https://doi.org/10.1017/jfm.2017.94

Andrews, B. J., & Befus, K. S. (2020). Supersaturation nucleation and growth of plagioclase: A numerical model of decompression-induced crystallization. *Contributions to Mineralogy and Petrology*, *175*(3), 1–20. https://doi.org/10.1007/s00410-020-1660-9

Annen, C., Blundy, J., & Sparks, R. (2005). The Genesis of intermediate and silicic magmas in deep crustal hot zones. *Journal of Petrology*, *47*(3), 505–539. https://doi.org/10.1093/petrology/egi084

Bachmann, O., Dungan, M. A., & Lipman, P. W. (2002). The fish canyon magma body, san juan volcanic field, Colorado: Rejuvenation and eruption of an upper-crustal batholith. *Journal of Petrology*, *43*(8), 1469–1503. https://doi.org/10.1093/petrology/43.8.1469

Barbey, P., Gasquet, D., Pin, C., & Bourgeix, A. L. (2008). Igneous banding, schlieren and mafic enclaves in calc-alkaline granites: The Budduso pluton (Sardinia). *Lithos*, *104*(1–4), 147–163. https://doi.org/10.1016/j.lithos.2007.12.004

Batchelor, C. K., & Batchelor, G. (2000). *An introduction to fluid dynamics*. Cambridge university press.

Befus, K. S., & Andrews, B. J. (2018). Crystal nucleation and growth produced by continuous decompression of pinatubo magma. *Contributions to Mineralogy and Petrology*, *173*(11), 1–20. https://doi.org/10.1007/s00410-018-1519-5

Bergantz, G., Schleicher, J., & Burgisser, A. (2015). Open-system dynamics and mixing in magma mushes. *Nature Geoscience*, *8*(10), 793–796. https://doi.org/10.1038/ngeo2534

Bergantz, G., Schleicher, J., & Burgisser, A. (2017). On the kinematics and dynamics of crystal-rich systems. *Journal of Geophysical Research: Solid Earth*, *122*(8), 6131–6159. https://doi.org/10.1002/2017jb014218

Bergé, P., & Dubois, M. (1984). Rayleigh-bénard convection. *Contemporary Physics*, *25*(6), 535–582. https://doi.org/10.1080/00107518408210730

Blundy, J., Cashman, K., & Humphreys, M. (2006). Magma heating by decompression-driven crystallization beneath andesite volcanoes. *Nature*, *443*(7107), 76–80. https://doi.org/10.1038/nature05100

Brandeis, G., & Jaupart, C. (1987). The kinetics of nucleation and crystal growth and scaling laws for magmatic crystallization. *Contributions to Mineralogy and Petrology*, *96*(1), 24–34. https://doi.org/10.1007/bf00375522

Browne, B. L., Eichelberger, J. C., Patino, L. C., Vogel, T. A., Dehn, J., Uto, K., & Hoshizumi, H. (2006). Generation of Porphyritic and Equigranular mafic enclaves during magma recharge events at Unzen volcano, Japan. *Journal of Petrology*, *47*(2), 301–328. https://doi.org/10.1093/petrology/egi076

Broxton, D. E., Warren, R. G., Byers, F. M., & Scott, R. B. (1989). Chemical and mineralogic trends within the timber mountain-Oasis valley caldera complex, Nevada: Evidence for multiple cycles of chemical evolution in a long-lived silicic magma system. *Journal of Geophysical Research*, *94*(10), 5961–5985. https://doi.org/10.1029/JB094iB05p05961

Burgisser, A., Bergantz, G. W., & Breidenthal, R. E. (2005). Addressing complexity in laboratory experiments: The scaling of dilute multiphase flows in magmatic systems. *Journal of Volcanology and Geothermal Research*, *141*(3–4), 245–265. https://doi.org/10.1016/j.jvolgeores.2004.11.001

Burns, P., & Meiburg, E. (2015). Sediment-laden fresh water above salt water: Nonlinear simulations. *Journal of Fluid Mechanics*, *762*, 156–195. https://doi.org/10.1017/jfm.2011.474

Cashman, K., & Blundy, J. (2013). Petrological cannibalism: The chemical and textural consequences of incremental magma body growth. *Contributions to Mineralogy and Petrology*, *166*(3), 703–729. https://doi.org/10.1007/s00410-013-0895-0

Cashman, K., Sparks, R., & Blundy, J. (2017). Vertically extensive and unstable magmatic systems: A unified view of igneous processes. *Science*, *355*(6331), eaag3055. https://doi.org/10.1126/science.aag3055

Chandrasekhar, S. (2013). *Hydrodynamic and hydromagnetic stability*. Courier Corporation.

Cheng, L., Costa, F., & Bergantz, G. (2020). Linking fluid dynamics and olivine crystal scale zoning during simulated magma intrusion. *Contributions to Mineralogy and Petrology*, *175*(6). https://doi.org/10.1007/s00410-020-01691-3

Cooper, K. M., & Kent, A. J. (2014). Rapid remobilization of magmatic crystals kept in cold storage. *Nature*, *506*(7489), 480–483. https://doi.org/10.1038/nature12991

Couch, S., Sparks, R., & Carroll, M. R. (2001). Mineral disequilibrium in lavas explained by convective self-mixing in open magma chambers. *Nature*, *411*(6841), 1037–1039. https://doi.org/10.1038/35082540

Culha, C. (2022). *Fluid and Thermodynamic Simulator of Magmatic Systems*. Retrieved from https://doi.org/10.5281/zenodo.6482286

Culha, C., Suckale, J., Keller, T., & Qin, Z. (2020). Crystal fractionation by crystal-driven convection. *Geophysical Research Letters*, *47*(4), e2019GL086784. https://doi.org/10.1029/2019GL086784

Davidson, J. P., & Tepley, F. J. (1997). Recharge in volcanic systems: Evidence from isotope profiles of phenocrysts. *Science*, *275*(5301), 826–829. https://doi.org/10.1126/science.275.5301.826

Demouchy, S., & Mackwell, S. (2006). Mechanisms of hydrogen incorporation and diffusion in iron-bearing olivine. *Physics and Chemistry of Minerals*, *33*(5), 347–355. https://doi.org/10.1007/s00269-006-0081-2

DiBenedetto, M., Qin, Z., & Suckale, J. (2020). Crystal aggregates record the pre-eruptive flow field in the volcanic conduit at kīlauea, Hawaii. *Science Advances*, *6*(49), eabd4850. https://doi.org/10.1126/sciadv.abd4850

Donaldson, C. (1985). A comment on crystal shapes resulting from dissolution in magmas. *Mineralogical Magazine*, *49*(350), 129–132. https://doi.org/10.1180/minmag.1985.049.350.19

Drazin, P. G., & Reid, W. H. (2004). *Hydrodynamic stability*. Cambridge university press.

Dufek, J., & Bachmann, O. (2010). Quantum magmatism: Magmatic compositional gaps generated by melt-crystal dynamics. *Geology*, *38*(8), 687–690. https://doi.org/10.1130/g30831.1

Dufek, J., & Bergantz, G. (2005). Transient two-dimensional dynamics in the upper conduit of a rhyolitic eruption: A comparison of closure models for the granular stress. *Journal of Volcanology and Geothermal Research*, *143*(1–3), 113–132. https://doi.org/10.1016/j.jvolgeores.2004.09.013

Flynn, L. P., & Mouginis-Mark, P. J. (1994). Temperature of an active lava channel from spectral measurements, kilauea volcano, Hawaii. *Bulletin of Volcanology*, *56*(4), 297–301. https://doi.org/10.1007/bf00302082

Garcia, M. O., & Jacobson, S. S. (1979). Crystal clots, amphibole fractionation and the evolution of calc-alkaline magmas. *Contributions to Mineralogy and Petrology*, *69*(4), 319–327. https://doi.org/10.1007/bf00372257

Ghiorso, M. S., & Gualda, G. A. R. (2015). An H_2O â CO_2 mixed fluid saturation model compatible with rhyolite â MELTS. *Contributions to Mineralogy and Petrology*, *169*(6), 1–30. https://doi.org/10.1007/s00410-015-1141-8

Ginibre, C., Wörner, G., & Kronz, A. (2007). Crystal zoning as an archive for magma evolution. *Elements*, *3*(4), 261–266. https://doi.org/10.2113/gselements.3.4.261

Gualda, G. A. R., Ghiorso, M. S., Lemons, R. V., & Carley, T. L. (2012). Rhyolite-MELTS: A modified calibration of MELTS optimized for silica-rich, fluid-bearing magmatic systems. *Journal of Petrology*, *53*(5), 875–890. https://doi.org/10.1093/petrology/egr080

Huber, C., Bachmann, O., & Manga, M. (2009). Homogenization processes in silicic magma chambers by stirring and mushification (latent heat buffering). *Earth and Planetary Science Letters*, *283*(1–4), 38–47. https://doi.org/10.1016/j.epsl.2009.03.029

Huppert, H. E., & Sparks, R. (1988). The generation of granitic magmas by intrusion of basalt into continental crust. *Journal of Petrology*, *29*(3), 599–624. https://doi.org/10.1093/petrology/29.3.599

Irvine, T. (1980). Magmatic density currents and cumulus processes. *American Journal of Science*, *280*, 1–58.

Jackson, E. (1961). Primary textures and mineral associations in the ultramafic zone of the stillwater complex, Montana: Us geol. survey prof. *Sec*, *1*, 135–140. paper 358, 106 p. 1963, chromium. 23rd Session.

Kahl, M., Chakraborty, S., Costa, F., & Pompilio, M. (2011). Dynamic plumbing system beneath volcanoes revealed by kinetic modeling, and the connection to monitoring data: An example from mt. etna. *Earth and Planetary Science Letters*, *308*(1–2), 11–22. https://doi.org/10.1016/j.epsl.2011.05.008

Keller, T., Katz, R. F., & Hirschmann, M. M. (2017). Volatiles beneath mid-ocean ridges: Deep melting, channelised transport, focusing, and metasomatism. *Earth and Planetary Science Letters*, *464*, 55–68. https://doi.org/10.1016/j.epsl.2017.02.006

Keller, T., & Suckale, J. (2019). A continuum model of multi-phase reactive transport in igneous systems. *Geophysical Journal International*, *219*(1), 185–222. https://doi.org/10.1093/gji/ggz287

Kerr, R. C. (1995). Convective crystal dissolution. *Contributions to Mineralogy and Petrology*, *121*(3), 237–246. https://doi.org/10.1007/bf02688239

Lamb, H. (1911). Xv. on the uniform motion of a sphere through a viscous fluid. *The London, Edinburgh, and Dublin Philosophical Magazine and Journal of Science*, *21*(121), 112–121. https://doi.org/10.1080/14786440108637012

Mittal, T., & Richards, M. A. (2017). Plume-ridge interaction via melt channelization at g alápagos and other near-ridge hotspot provinces. *Geochemistry, Geophysics, Geosystems*, *18*(4), 1711–1738. https://doi.org/10.1002/2016gc006454

Mucha, P. J., Tee, S. Y., Weitz, D. A., Shraiman, B. I., & Brenner, M. P. (2004). A model for velocity fluctuations in sedimentation. *Journal of Fluid Mechanics*, *501*(501), 71–104. https://doi.org/10.1017/S0022112003006967

Murphy, M., Sparks, R., Barclay, J., Carroll, M., & Brewer, T. (2000). Remobilization of andesite magma by intrusion of mafic magma at the soufriere hills volcano, Montserrat, west indies. *Journal of Petrology*, *41*(1), 21–42. https://doi.org/10.1093/petrology/41.1.21

Qin, Z., Allison, K., & Suckale, J. (2020). Direct numerical simulations of viscous suspensions with variably shaped crystals. *Journal of Computational Physics*, *401*, 109021. https://doi.org/10.1016/j.jcp.2019.109021

Qin, Z., & Suckale, J. (2016). A virtual laboratory for three-phase flow: 1. *Direct numerical simulations of bubble-crystal interactions in basaltic suspensions*, *1–60*.

Qin, Z., & Suckale, J. (2017). Direct numerical simulations of gasâsolidâliquid interactions in dilute fluids. *International Journal of Multiphase Flow*, *96*(November), 34–47. https://doi.org/10.1016/j.ijmultiphaseflow.2017.07.008

Qin, Z., & Suckale, J. (2020). Flow-to-sliding transition in crystal-bearing magma. *Journal of Geophysical Research: Solid Earth*, *125*(2), e2019JB018549. https://doi.org/10.1029/2019jb018549

Rae, A. S. P., Edmonds, M., Maclennan, J., Morgan, D., Houghton, B., Hartley, M. E., & Sides, I. (2016). Time scales of magma transport and mixing at K??lauea Volcano, Hawai'i. *Geology*, *44*(6), 463–466. https://doi.org/10.1130/G37800.1

Rayleigh, L. (1883). Investigation of the character of the equilibrium of an incompressible heavy fluid of variable density. *Proceedings of the London Mathematical Society*, *14*(39), 170–177.

Rubin, A. E., Cooper, K. M., Till, C. B., Kent, A. J., Costa, F., Bose, M., et al. (2017). Rapid cooling and cold storage in a silicic magma reservoir recorded in individual crystals. *Science*, *356*(6343), 1154–1156. https://doi.org/10.1126/science.aam8720

Ruth, D. C., Costa, F., De Maisonneuve, C. B., Franco, L., Cortés, J. A., & Calder, E. S. (2018). Crystal and melt inclusion timescales reveal the evolution of magma migration before eruption. *Nature Communications*, *9*(1), 1–9. https://doi.org/10.1038/s41467-018-05086-8

Schwindinger, K. R., & Anderson, A. T. Jr. (1989). Synneusis of kilauea Iki olivines. *Contributions of Mineralogy and Petrology*, *103*, 187—198. https://doi.org/10.1007/bf00378504

Segre, P. N., Liu, F., Umbanhowar, P., & Weitz, D. A. (2001). An effective gravitational temperature for sedimentation. *Nature*, *409*(February), 594–597. https://doi.org/10.1038/35054518

Shane, P., & Smith, V. C. (2013). Using amphibole crystals to reconstruct magma storage temperatures and pressures for the post-caldera collapse volcanism at Okataina volcano. *Lithos*, *156*, 159–170. https://doi.org/10.1016/j.lithos.2012.11.008

Singer, B. S., Dungan, M. A., & Layne, G. D. (1995). Textures and Sr, Ba, Mg, Fe, K, and Ti compositional profiles in volcanic plagioclase: Clues to the dynamics of calc-alkaline magma chambers. *American Mineralogist*, *80*, 776–798. https://doi.org/10.2138/am-1995-7-815

Sparks, S. R. J., Sigurdsson, H., & Wilson, L. (1977). Magma mixing: A mechanism for triggering acid explosive eruptions. *Nature*, *267*(5609), 315–318. https://doi.org/10.1038/267315a0

Spilliaert, N., Allard, P., Métrich, N., & Sobolev, A. (2006). Melt inclusion record of the conditions of ascent, degassing, and extrusion of volatile-rich alkali basalt during the powerful 2002 flank eruption of Mount Etna (Italy). *Journal of Geophysical Research*, *111*(B4). https://doi.org/10.1029/2005jb003934

Suckale, J., Sethian, J., Yu, J., & Elkins-Tanton, L. (2012). Crystals stirred up: 1. Direct numerical simulations of crystal settling in nondilute magmatic suspensions. *Journal of Geophysical Research*, *117*(8). https://doi.org/10.1029/2012JE004066

Toramaru, A. (2001). A numerical experiment of crystallization for a binary eutectic system with application to igneous textures. *Journal of Geophysical Research*, *106*(B3), 4037–4060. https://doi.org/10.1029/2000jb900367

Vogt, J. H. L. (1921). The physical chemistry of the crystallization and magmatic differentiation of igneous rocks. *The Journal of Geology*, *29*(4), 318–350. https://doi.org/10.1086/622785

Waight, T. E., Maas, R., & Nicholls, I. A. (2000). Fingerprinting feldstar phenocrysts using crystal isotopic composition stratigraphy: Implications for crystal transfer and magma mingling in S-type granites. *Contributions to Mineralogy and Petrology*, *139*(2), 227–239. https://doi.org/10.1007/s004100000128

Wallace, G. S., & Bergantz, G. W. (2005). Reconciling heterogeneity in crystal zoning data: An application of shared characteristic diagrams at Chaos Crags. Lassen Volcanic Center, California. *Contributions to Mineralogy and Petrology*. https://doi.org/10.1007/s00410-004-0639-2

Whitney, J. A., & Stormer, J. C. (1985). Mineralogy, petrology, and magmatic conditions from the fish canyon tuff, central san juan volcanic field, Colorado. *Journal of Petrology*, *26*(3), 726–762. https://doi.org/10.1093/petrology/26.3.726

Zellmer, G., Sparks, R., Hawkesworth, C., & Wiedenbeck, M. (2003). Magma emplacement and remobilization timescales beneath Montserrat: Insights from sr and ba zonation in plagioclase phenocrysts. *Journal of Petrology*, *44*(8), 1413–1431. https://doi.org/10.1093/petrology/44.8.1413